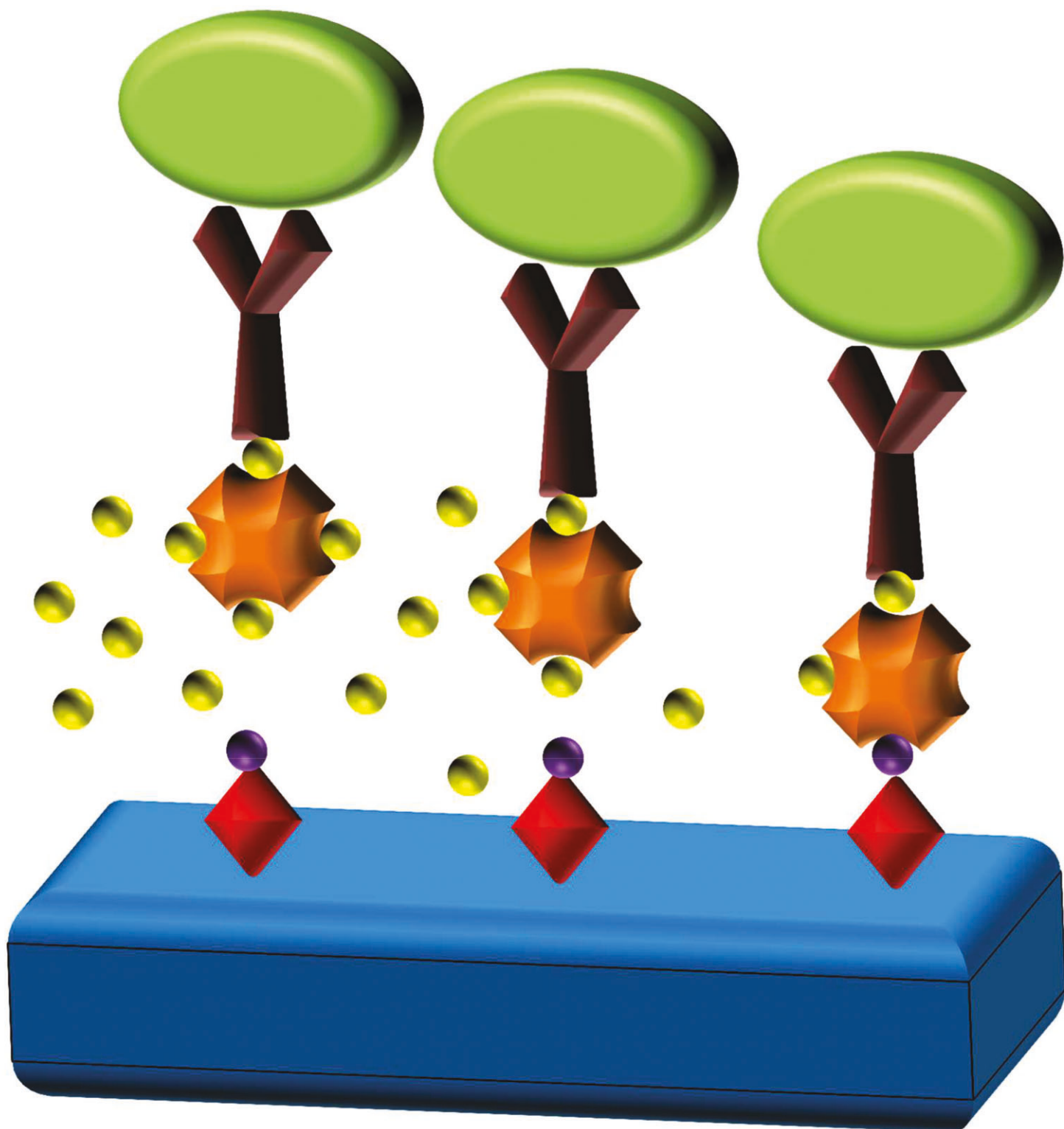


# BIOTECHNOLOGY *and* BIOENGINEERING

VOLUME 112 NUMBER 11 NOVEMBER, 2015



## Secondary Anchor Targeted Cell Release

Ali Ansari, Felipe T. Lee-Montiel, Jennifer R. Amos, P. I. Imoukhuede

Department of Bioengineering, University of Illinois at Urbana Champaign, Urbana, Illinois 61801; telephone: +1217-244-2651; e-mail: pii@illinois.edu

**ABSTRACT:** Personalized medicine offers the promise of tailoring therapy to patients, based on their cellular biomarkers. To achieve this goal, cellular profiling systems are needed that can quickly and efficiently isolate specific cell types without disrupting cellular biomarkers. Here we describe the development of a unique platform that facilitates gentle cell capture via a secondary, surface-anchoring moiety, and cell release. The cellular capture system consists of a glass surface functionalized with APTES, d-desthiobiotin, and streptavidin. Biotinylated mCD11b and hIgG antibodies are used to capture mouse macrophages (RAW 264.7) and human breast cancer (MCF7-GFP) cell lines, respectively. The surface functionalization is optimized by altering assay components, such as streptavidin, d-desthiobiotin, and APTES, to achieve cell capture on 80% of the functionalized surface and cell release upon biotin treatment. We also demonstrate an ability to capture 50% of target cells within a dual-cell mixture. This engineering advancement is a critical step towards achieving cell isolation platforms for personalized medicine.

Biotechnol. Bioeng. 2015;112: 2214–2226.

© 2015 Wiley Periodicals, Inc.

**KEYWORDS:** cell isolation; personalized medicine; desthiobiotin; streptavidin; glass functionalization; APTES

The leading cancer research foundations (e.g., ACS, NCI, AACR) have identified personalized medicine as a critical need in advancing cancer treatment (Doroshov, 2009; Salwitz, 2012; Hansen, 2015). Personalized medicine offers the ability to tailor therapy to patients based on their distribution of cell-surface receptors on specific cells within a tissue (Chen et al., 2014). Indeed, by applying quantitative

flow (qFlow) cytometry (Chen et al., 2015), we recently showed that variability in cell-surface vascular endothelial growth factors can mathematically define tumor endothelial cell subpopulations from breast cancer xenografts (Imoukhuede and Popel, 2014). We computationally predicted how these tumor-associated cell subpopulations would elicit differing Avastin, therapeutic response (Weddell and Imoukhuede, 2014)—accordingly, isolating and profiling tumor and tumor-associated cells could offer a new approach for personalized prediction of Avastin and other anti-angiogenic therapeutic responsiveness (Weddell and Imoukhuede, 2014). In addition to improved understanding of tumor angiogenesis, cell isolation would also have clinical applications to other cancer diagnostics, (Cristofanilli et al., 2004; Gascoyne et al., 2009; Arya et al., 2013) and stem cell research (Asahara et al., 1997; Ferrara and Kerbel, 2005; De Coppi et al., 2007; Kelly et al., 2011).

In order to achieve the promise of personalized medicine profiling, systems are needed that can quickly, and efficiently isolate specific cell types without disrupting cell-surface receptor-levels. The “lab on a chip” concept offers the promise of  $>100\times$  faster (hour-to-minute) cell isolation. Some novel approaches include optical trapping (Mishra et al., 2014; Roxworthy et al., 2014), microfluidics (Cheung et al., 2009; Liu et al., 2010; He et al., 2015), and surface functionalization (Park et al., 2007; Plouffe et al., 2009; Sheng et al., 2014). While, these approaches offer the advantages of sensing protein (Schudel et al., 2009; Galletti et al., 2014) or RNA expression (Lien et al., 2010; Stott et al., 2010; Yu et al., 2012) or providing cells for in vitro culture (Zheng et al., 2011; Sheng et al., 2014), many cannot be applied towards the quantitative profiling of cell-surface receptors, because they cause irreversible damage to cells. Indeed, fluid shear forces, as low as 0.5–5 Pa, can trigger necrosis or cell fracture (Tanzeglock et al., 2009) and mild chemical digestion (e.g., collagenases, trypsin) can cleave cell-surface receptors (Imoukhuede and Popel, 2011,2012), while cell lysis renders cell-surface receptors indistinguishable from intracellular receptors (Ludwig et al., 1992). New methods are therefore needed to capture and release endothelial cells while preserving cell surface-receptor levels.

Here we present a new method of secondary anchor targeted cell release that should preserve cell structure and function. The primary anchor, a biotinylated antibody, binds to cells and the secondary anchor, a streptavidin (SAv)—d-desthiobiotin (DSB) (reversible)—functionalized surface, is targeted for cell release through biotin competition ( $K_d$  desthiobiotin-streptavidin =  $10^{-13}$ ,  $K_d$  biotin-streptavidin =  $10^{-15}$ ) (Hoffmann et al., 1992; Qureshi and Wong, 2002; Magalhães et al., 2011). DSB is a biotin analogue that differs from biotin in that it lacks one sulfur group, resulting in a

Ali Ansari and Felipe T. Lee-Montiel contributed equally.

Author Contributions: F.L.M. conceived this research project. A.A., P.I.I. and F.L.M analyzed the results and wrote the manuscript. F.L.M. and A.A. designed and carried out experiments. J.A. helped analyze AFM image and data analysis. All authors have given approval to the final version of the manuscript.

Present addresses of Felipe T. Lee-Montiel is University of Pittsburgh, Drug Discovery Institute, 10040 Biomedical Science Tower 3, 3501 Fifth Avenue, Pittsburgh, PA 15260. Abbreviations: CCR2, CC chemokine receptor 2; CCL2, CC chemokine ligand 2; CCR5, CC chemokine receptor 5; TLC, thin layer chromatography, DSB Desthiobiotin, Qdot (Quantum dot).

Correspondence to: P.I. Imoukhuede

Contract grant sponsor: American Cancer Society

Contract grant sponsor: Illinois Division Basic Research Grant

Contract grant sponsor: Mexico's National Council of Science and Technology (CONACyT)

Received 22 December 2014; Accepted 11 May 2015

Accepted manuscript online 22 May 2015;

Article first published online in Wiley Online Library

(<http://onlinelibrary.wiley.com/doi/10.1002/bit.25648/abstract>).

DOI 10.1002/bit.25648

100-fold decrease in its affinity for SAV and is easily displaced by biotin. The interaction between DSB and SAV is used to pull-down cells, and the competing interaction of excess biotin replaces the DSB, resulting in the passive release of the capture surface without additional force.

We identify optimal conditions for surface functionalization by varying and analyzing surface properties. We demonstrate SAV-Quantum dots (SAV-Qdots) capture and release, MCF7-GFP capture and release, and selective capture and release of RAW 264.7 (mouse macrophage cell line) from a dual-cell mixture. This new method provides an effective cell capture and release that can be applied to isolate target cells from multi-cell samples.

## MATERIALS AND METHODS

### Concept

The cellular capture system consists of a functionalized glass surface involving four major layers: (3-Aminopropyl) triethoxysilane (APTES); DSB (for reversible binding to SAV); SAV; and a cell-specific biotinylated antibody (Fig. 1). The cells are captured by the antibodies on this surface and released via introduction of excess biotin, which competes with the DSB.

### Surface Functionalization

Several glass surfaces were used: an uncoated 8-well culture slide (BD Falcon, San Jose, California), plain microscope slides (Corning, Catalog number 2947-75 × 38, Tewksbury, MA), microscope cover slides (Thermo Scientific, Catalog Number 22 × 70, Waltham, MA), Lab-Tek II 8-well slides (Nunc/Thermo Scientific, Catalog Number 154534, Pittsburgh, PA), and Glass bottom P24G-0-13-F, 24-well plates (MatTek, Ashland, MA). Glass was cleaned using Diener Plasma Cleaner Pico (Royal Oak, MI) for 5 min at 50% power. 2% (3-Aminopropyl) triethoxysilane (APTES) (Acros Organics, Geel, Belgium) in ethanol was applied to the oxygen plasma cleaned glass surface for 50 min and cured in a Thermo Scientific Precision Oven (Thermo Scientific, Pittsburg, PA) for 2 h at 55°C. d-Desthiobiotin (DSB) (Sigma, St. Louis, MO) was solubilized with 10 μL dimethyl sulfoxide (BDH, Radnor, PA) per mg of DSB. The DSB carbonyl group at 1.5 mg/mL was activated and combined with 1-Ethyl-3-(3-dimethylaminopropyl) carbodiimide (EDC) (Thermo Scientific, Pittsburg, PA). The activated DSB was dissolved in pH 6.0, 2-(N-morpholino) ethanesulfonic acid (MES buffer) for 15 min and quenched using mercaptoethanol. Following overnight incubation at 4°C in a refrigerator, excess DSB was washed with phosphate buffered saline (PBS) three times and 0.4 mg/mL streptavidin (Proteochem, Loves Park, IL) in PBS was applied overnight at 4°C,

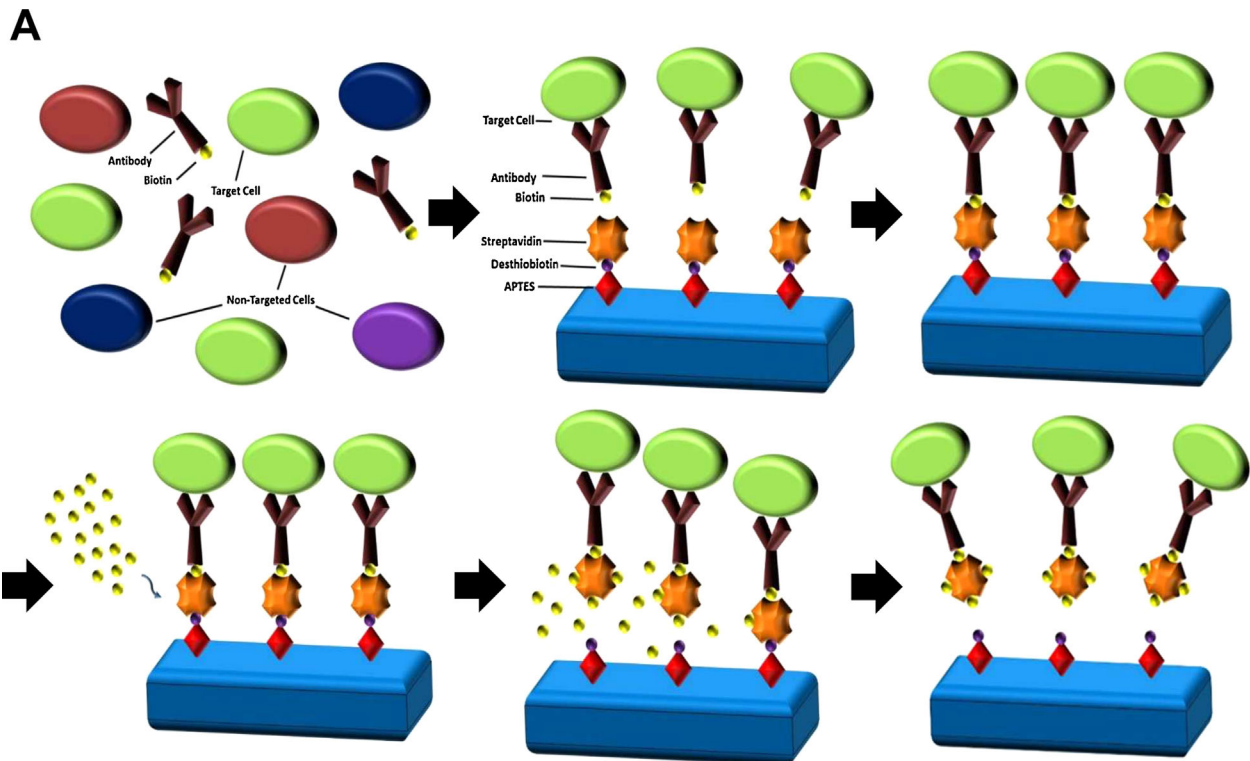


**Figure 1.** Schematic of surface functionalization for cell isolation. Glass surface functionalized with (3-Aminopropyl) triethoxysilane (APTES), a self-assembling silane that allows for an amine from which subsequent layers can be attached to the glass; DSB which allows for reversible binding to SAV and is the crux of the release mechanism for the cells; SAV which serves as the adaptor that allows for cellular conjugation to the floor; and a cell-specific biotinylated antibody which serves as the differentiation mechanism for the sorting of the cells. The SAV-antibody-cell complex is released via the introduction of excess biotin, which competes with DSB-SAV binding ( $K_{d, \text{desthiobiotin-streptavidin}} = K_{d, \text{biotin-streptavidin}} = 10^{-13}$ ). This competition releases the DSB and replaces it with the more strongly bound biotin. This releases the entire cell-antibody-SAV complex from the functionalized surface, allowing for collection.

rinsed with PBS, rewetted, and replaced in the refrigerator until use. This protocol was modified from (Caicedo et al., 2012).

## Cell Culture

MCF7-GFP cells, a luminal breast cancer cell line, were obtained from Cell Biolabs (San Diego, CA). MCF7-GFP cells were grown in high glucose Dulbecco's modified Eagle medium (DMEM) supplemented with nonessential amino acids (University of Illinois Cell Media Facility, School of Chemical Sciences, Urbana, IL), 10% fetal bovine serum (Invitrogen, Carlsbad, CA), and 1% Penicillin–Streptomycin (Invitrogen). The RAW 264.7 mouse macrophages were gifted to us from the Smith lab at the University of Illinois. RAW 264.7 cells were grown in DMEM containing 10% fetal bovine serum and 1% penicillin-streptomycin. All cells were maintained at 37°C in 95% air, 5% CO<sub>2</sub>. Cells were grown to confluence before the experiment. For routine cell passaging, cells were detached from flasks using TrypLe (Life Technologies, Carlsbad, CA). For capture experiments, CellStripper cell dissociation solution (Corning, Manassas, VA) was applied for 5–7 min at 37°C. Cells were re-suspended in 10 mL stain buffer, which contains from PBS with 1% BSA and 0.09% sodium azide. Cells were centrifuged at 500g for 5 min at 4°C, the supernatant aspirated, and cells re-suspended in cold Hanks Balanced Salt Solution without calcium, magnesium, or phenol red to a final concentration of  $1 \times 10^6$  cells/mL.

## Antibody biotinylation

Antibodies were biotinylated at a concentration of 0.5 mg hIgG/mL or 1 mg mCD11b/mL using the EZ-Link Sulfo-NHS-LC Biotinylation Kit (Thermo Scientific, Waltham, MA), following the manufacturer's instructions. Briefly, antibody was incubated with Sulfo-NHS linked biotin for 2 h. Biotinylated antibody was purified with Zeba Spin Desalting columns (Thermo Scientific, Waltham, MA) and centrifuged at 1000g for 2 min. For small-volume samples, a stacker was applied, ensuring complete sample flow through the desalting column.

## Cell capture

MCF7-GFP cells were targeted with either by hIgG, HP6017 (BioLegend, San Diego, CA) or hHLA-A,B,C, 311402 (BioLegend, San Diego, CA) and RAW 264.7 cells were targeted with mCD11b, MA5-17826 (Thermo Scientific). The antibodies and the cells were incubated for 30 min at 4°C in an end-over-end mixer. The functionalized glass surfaces were uncoated 8-well plates that were initially washed with Hanks Balanced Salt Solution without calcium and without magnesium (HBSS) before incubation of cells. 300  $\mu$ L of cells concentrated to 1 million cells/mL (300,000 cells) were seeded in each well. Cells were incubated for 45 min on ice on a shaker. Following cell capture, surfaces were gently washed with 500  $\mu$ L HBSS and resuspended in 200  $\mu$ L HBSS (control) or released with 300  $\mu$ L of 20 mM biotin (Amresco, Solon, OH). After a 20 min shaking on ice, all wells were gently washed with HBSS 500  $\mu$ L HBSS and resuspended in 200  $\mu$ L HBSS.

## Fluorescence Microscopy

SAv-Qdots were seeded in a functionalized 8-well coverglass (Thermo Labtek II) and incubated for 45 min at 25°C to allow for SAv-Qdot-DSB attachment. Qdots were imaged on an inverted Zeiss LSM 710 Confocal Microscope at 8 bits using 5 channels and  $512 \times 512$  pixel resolution. Cells were excited with a 405 nm laser at 17–22% laser power using a 63 $\times$  apochromat 1.4 NA oil-immersion objective. Fluorescence was collected with the 32-channel Quasar multichannel photomultiplier tube. Wide-Field cell imaging was performed on a Zeiss Axiovert 200 M inverted fluorescence microscope in the Beckman Institute at the University of Illinois at Urbana-Champaign, using a 10 $\times$  Plan-Neofluar objective with a numerical aperture of 0.30 and a working distance of 5.6 mm in air. The Axiovert uses a 120 Hg UV lamp and imaged GFP fluorescence using the 470EX/515EM FITC Chroma Set 41025. Images were analyzed using the FIJI, Image J software package.

## Atomic Force Microscopy

All AFM measurements were performed in tapping mode on an Asylum Research MFP-3D AFM (Asylum Research, Santa Barbara, CA). The scan rate was 1 Hz, and 256 line resolution. The scan size was  $1 \times 1 \mu$ m. The scanning angle was 90°, the drive amplitude was 0.3166–0.37704, and the Drive frequency was 310,000. We used Tap300-G silicon tips from Budget Sensors (Sofia, Bulgaria) with a force constant of 40 N/m. Igor (WaveMetrics, Portland, OR) was used to analyze the raw AFM data and obtain the standard deviation data.

## Antibody and Cell Titration Studies

24-well plates (MatTek) were functionalized and then titrated across several different concentrations of cells and antibodies to find the optimum concentrations for both. For the antibody titration, five different concentrations of HLA-ABC antibodies, ranging from 1 to 10,000 ng/mL were used. MCF7-GFP cells at 1 million cells/mL were incubated on the surface for 45 min and gently washed any non-adherent cells. The 24-well plates were imaged on a Biotek Synergy HT Plate Reader (Biotek, Winooski, VT) at 485nm, 528 nm emission. Data were analyzed with OriginLab (Origin Corp, Northampton, MA) to determine the optimum antibody concentration of 10 ng/mL. We used the optimum concentration for cell titration, adding 10 ng/mL HLA-ABC or hIgG antibody to six different concentrations of MCF7-GFP cells, ranging from 10 to 1,000,000 cells/mL. After 45 min incubation, we gently washed any non-adherent cells and imaged MCF7-GFP fluorescence with the plate reader (Fig. 9).

## RESULTS

### Testing Uniformity of SAv Functionalization

To identify SAv concentrations and incubation times leading to optimal capture and uniformity, we imaged the Labtek II glass surface functionalized with APTES, DSB, and SAv; incubated with biotinylated-Qdots 605; and performed wide-field fluorescence

imaging. The 0.3 mg/mL SAV functionalization showed the lowest fluorescence intensity (Fig. 2A and B), suggesting that this lower SAV concentration did not enable optimal capture. Furthermore, we observed a large standard deviation in the fluorescence intensity, indicating non-uniform surface binding. 0.5 mg/mL SAV functionalization resulted in the highest Qdot fluorescence intensity, which indicates high-capture onto the surface. However, this condition also had the highest fluorescence standard deviation, indicating regions of aggregation rather than uniform surface coverage. The 0.4 mg/mL SAV functionalization displayed ~20% lower fluorescence intensity relative to the 0.5 mg/mL case; it gave greater uniformity in Qdot coverage compared to either 0.3 mg/mL or 0.5 mg/mL as calculated via a standard deviation in fluorescence coverage. Additionally, we tested SAV incubation time, which

showed that overnight incubation (18–20 h) resulted in 80% higher SAV-Qdots binding compared to 4 h incubation (Fig. 2C), indicating that cellular capture before overnight incubation was not optimized (Supplementary Fig. S1). Thus, the 0.4 mg/mL, incubated overnight SAV enabled both increased and uniform binding.

### Characterizing Functionalized Surface Uniformity

The glass cleaned with ethanol and DI water had a surface height standard deviation of 1.969 nm, which was 83% greater than the standard deviation of the glass cleaned with oxygen plasma (Table 1). Since the oxygen plasma cleaning resulted in a more uniform glass surface, we used this to treat all subsequently tested layers. The 2% APTES surface had a 7% lower standard deviation

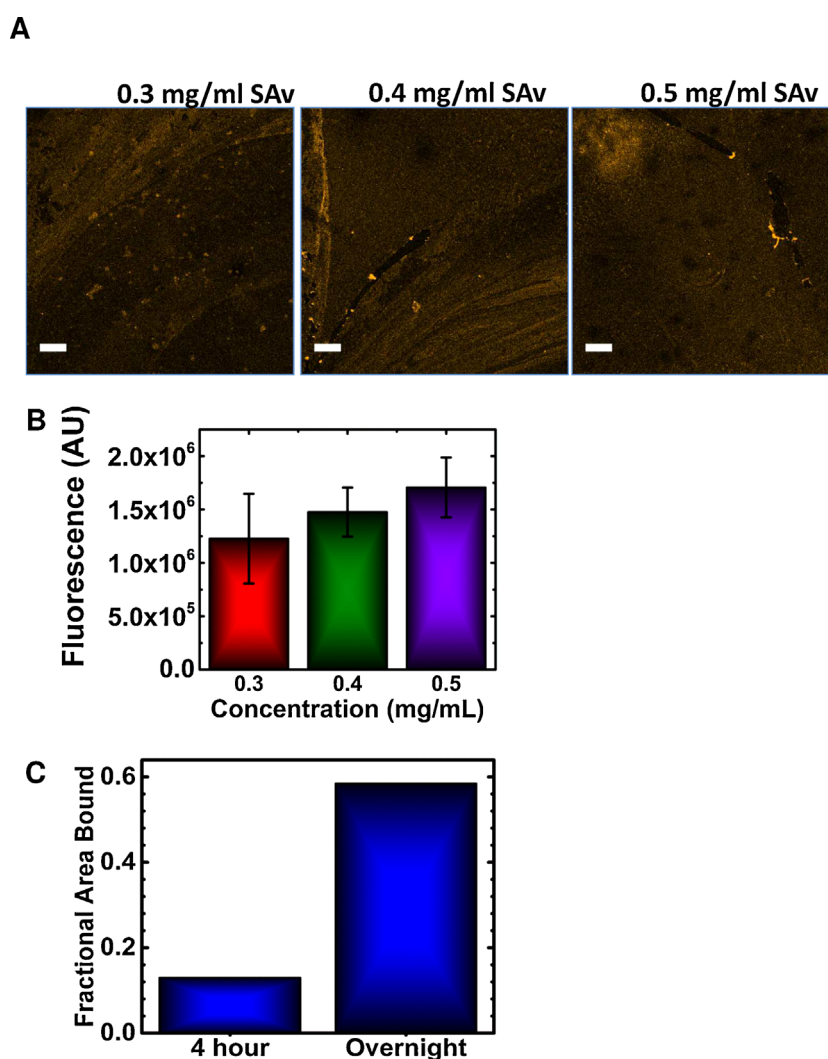


**Figure 2.** Visualizing capture of Qdots. (A) Surface functionalized with APTES, DSB, and 0.2 mg/mL, 0.3 mg/mL, and 0.4 mg/mL SAV was exposed to excess biotinylated Qdot 605. At 0.3 mg/mL SAV, there are large gaps in the fluorescently labeled areas, which show non-uniformity and incomplete functionalization of SAV. At 0.4 mg/mL, the fluorescence is much more uniform with a mostly complete coating, showing a more complete monolayering of SAV. At 0.5 mg/mL, the entire surface is functionalized non-uniformly resulting in much higher standard deviation in brightness despite more complete coverage, possibly due to multiple layering of SAV. Scale bar is 100 microns ( $\mu\text{m}$ ). (B) Quantitative graph illustrating the fluorescence profiles. (C) Cells binding to functionalized surfaces incubated with SAV overnight as compared to surfaces incubated with SAV for four hours, showing 4x higher fluorescent activity for overnight incubation.

**Table 1.** Igor-measured standard deviations of the different functionalized surfaces.

Functionalized surface	Standard deviation
Glass cleaned with ethanol and DI water	1.969 nm
Glass cleaned with oxygen plasma	1.078 nm
2% APTES functionalized glass	1.419 nm
5% APTES functionalized glass	1.332 nm
2% APTES, DSB, and functionalized glass	2.115 nm
5% APTES, DSB, and SAV functionalized glass	4.951 nm

than the 5% APTES surface, indicating that the 5% APTES surface was marginally more uniform than the 2% APTES surface. However, this trend was reversed in the comparison of fully functionalized 2% APTES, DSB, and SAV functionalized surface compared to the 5% APTES, DSB, and SAV functionalized surface. In the 2% fully functionalized surface, the standard deviation was 57% lower than the standard deviation for the 5% surface. Therefore, the 5% APTES fully functionalized surface was extremely non-uniform and not suitable as the basis of the capture surface. The 2% APTES fully functionalized surface was more uniform and thus became the basis for our capture surface.

### Characterizing Functionalized Surface Height

The functionalization of each layer affects subsequent layers, so significant variations can detrimentally affect cellular capture. We used atomic force microscopy (AFM) to image both a “dirty” (not-cleaned; Fig. 3A), and oxygen-plasma cleaned (Fig. 3B) glass surfaces modified with APTES. The dirty glass presented several non-homogenous regions (Fig. 3A), whereas, there was greater uniformity in the oxygen-plasma cleaned surface (Fig. 3B). When we examined the method of cleaning, we saw that cleaning with oxygen-plasma (Fig. 4B) had 2.5 nm less total height variation (from 3 nm to -2 nm), compared to ethanol, and water surface cleaning (from 3.5 nm to 0 nm; Fig. 3A and 4A). AFM imaging of the complete, functionalized surface showed a higher range of surface height when 5% APTES (Fig. 3F and 4F) was used, with surface heights ranging from -4 nm to 7 nm, compared with surface heights from 6 nm to -2 nm with 2% APTES (Fig. 3E and 4E). Altogether, our AFM imaging showed that oxygen-plasma cleaning followed by 2% APTES functionalization provided a more uniform surface.

### Calculating Shear Force on a SAV Bond

To determine whether our washing step could disrupt the DSB-SAV or the biotin-SAV bonds, we calculated the shear force that washing applied to these bonds. It was necessary to make several assumptions for this calculation. First, we assumed that the washing occurred as a one-dimensional flow parallel to the plate surface (Fig. 5). Initially, there was 1 mL of fluid within the well, the bottom of the well has an area of 0.7 cm<sup>2</sup>, and the washing step took approximately 2 s. This gave a volumetric flow rate of 0.5 mL/s within the well with a new fluid depth of 1.4 cm. Thus, the average fluid velocity across the glass plate/liquid interface was 0.42 cm/s. The shear stress was calculated at the

wall by:

$$\tau = \mu \left. \frac{dv}{dy} \right|_{y=0}$$

where  $\tau$  is the shear stress at the wall,  $\mu$  is the fluid viscosity,  $v$  is the fluid velocity, and  $y$  is the distance from the wall. We assumed the fluid viscosity is the same as water ( $\mu = 1 \text{ N} \cdot \text{s}/\text{m}^2$ ), that our average velocity occurred at the center of the fluid flow ( $dy = h/2 = 0.7 \text{ cm}$ ), and that there were no slip conditions along the bottom of the well plate ( $dv = 0.42 \text{ cm/s}$ ). This gave a shear stress at the plate interface of 0.6 N/m<sup>2</sup>. Assuming SAV is a sphere with a diameter of 5 nm (Kuzuya et al., 2008), the SAV surface area was 79 nm<sup>2</sup>. We further assumed that only the top half of SAV was exposed to fluid shear stress, making the available SAV surface area 39.5 nm<sup>2</sup>. Thus, we estimated that a single SAV bond experienced  $24 \times 10^{-6}$  pN of shear force. Prior research has shown that the force required to disrupt a biotin-avidin binding is 173 pN (Lee et al., 2007). While data on DSB-SAV disruption forces are not available, we predict that the disruption force would be in the 84–104 pN range, given that DSB-avidin coupling can be disrupted by forces of nearly half that of biotin-avidin (Lee et al., 2007). Overall, these calculations indicate that the wash steps in the experiment were unlikely to shear either the SAV and DSB bond or the SAV and biotin bond.

### Capture and release—Cells & Qdots

We examined the feasibility of biotin-mediated release by imaging SAV-Qdots 605 incubated on the functionalized surface (Fig. 2). We observed capture (Fig. 2A) and release via 20 min incubation with 20 mM biotin. When we extended this analysis to cells, we observed that biotinylated hIgG-bound to human MCF7-GFP cells were captured by our surface (Fig. 6A), resulting in 60% cell pull-down. When exposed to a controlled wash to eliminate non-specific adhesion, 50% of the cells were retained on the capture surface. The non-functionalized glass surfaces resulted in 70% pull down of cells but the binding was nearly all-nonspecific as after a controlled wash, only 15% of the cells remained. This indicates an effective capture surface. Twenty minutes 20 mM biotin treatment released ~80% of captured MCF7-GFP cells, whereas HBSS wash treatment released only 60% of attached cells.

### Capture and release—Cells within a mixture

We examined the ability of the surface and antibodies to isolate target cells by introducing a dual-cell population containing human breast cancer cells (MCF7-GFP) and mouse macrophages (RAW 264.7), and we used mCD11b, an antibody specific to the mouse macrophages, to selectively capture the macrophages. We chose these cell-types (primary tumor and immune) because they represent prevalent cells types in tumor biopsies (Mantovani et al., 2002; Murdoch et al., 2004) and murine xenograft models (Drews-Elger et al., 2014). Therefore, selective capture would be useful for future applications of this technology. Additionally, the fluorescent MCF7-GFP allowed cells to be readily imaged. We observed some non-specific adhesion of

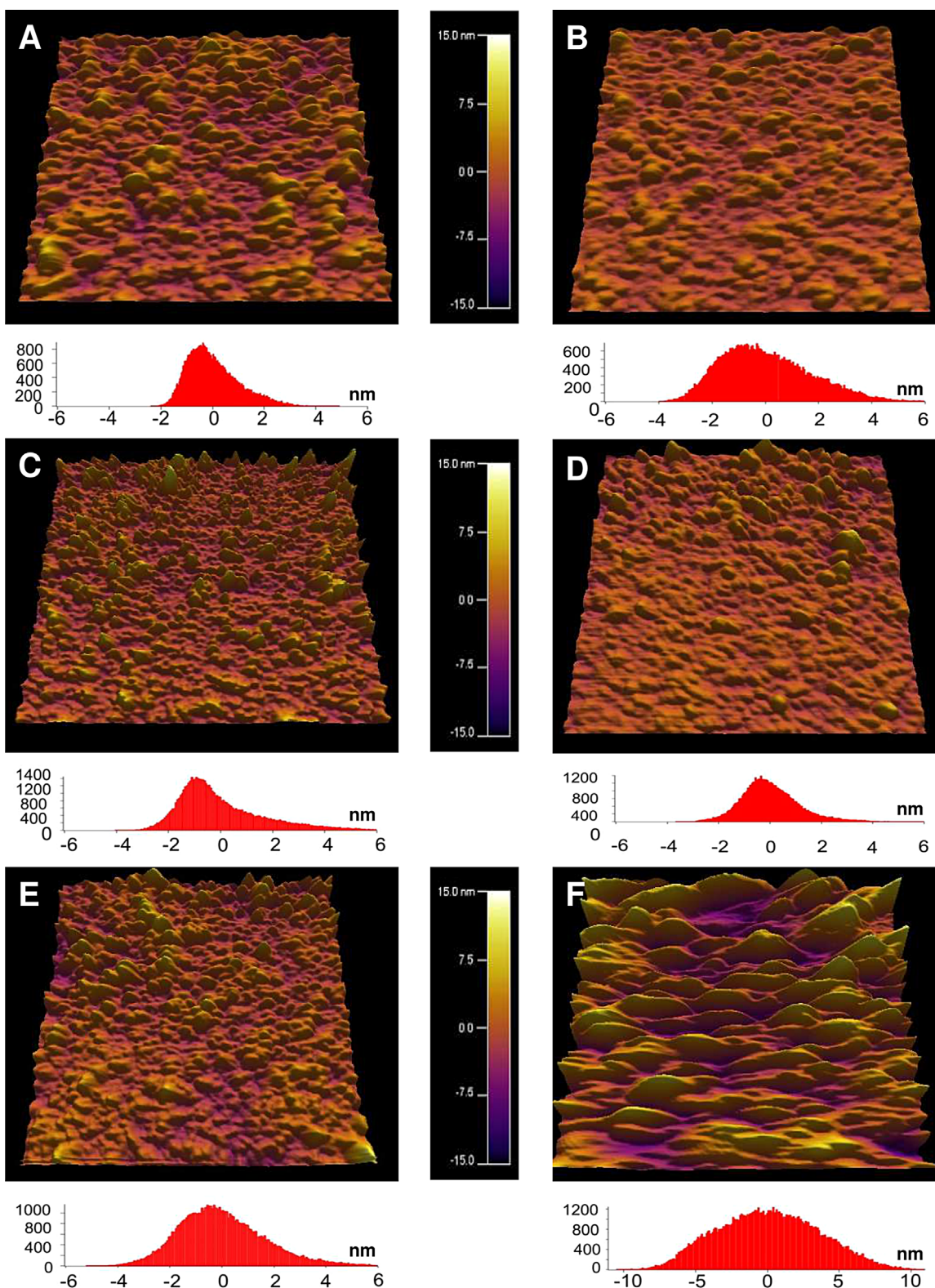


**Figure 3.** AFM Images of functionalized surfaces and surface height distribution. (A) Ethanol and DI water cleaned glass shows relative heterogeneity on the surface. (B) Oxygen Plasma Cleaned glass (C) Oxygen Plasma Cleaned glass functionalized with 2% APTES, (D) and with 5% APTES show the differences in both the uniformity and the height of the surfaces. (E) Glass functionalized with 2% APTES + DSB and (F) Glass functionalized with 5% APTES + DSB, and SAV show the drastic differences in layering as a result of the changes in the initial APTES layer concentration. The surfaces that have the smaller widths in the distributions are more uniformly distributed. The 5% APTES DSB, and SAV surface has substantially larger a distribution than the other surfaces, and as such has larger bounds than the rest of the surfaces.

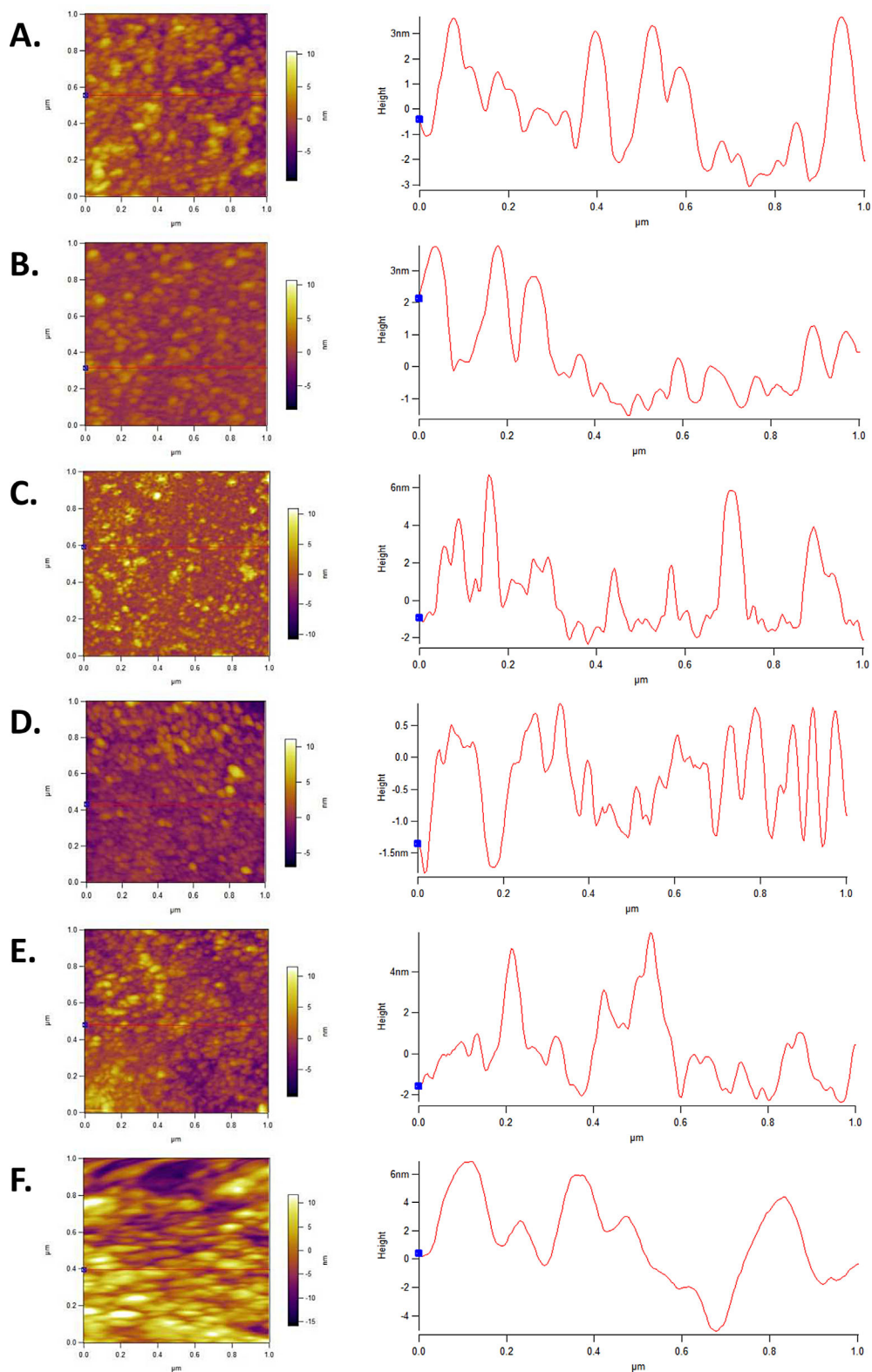


**Figure 4.** AFM Images of plain, oxygen plasma cleaned, APTES, and SAV functionalized glass surfaces with corresponding height measurements. Regular glass cleaned with ethanol and DI water (A) as compared to oxygen plasma cleaned glass (B). The heights shown below correspond to the heights sampled across the red line above. This shows that oxygen plasma cleaned glass is much more uniform than regular glass. Two percent APTES functionalized glass (C) as compared to 5% APTES functionalized glass (D). Both glass surfaces were initially oxygen plasma cleaned prior to functionalization. The heights shown below correspond to the heights sampled across the red line above. This shows that 5% APTES seems to be slightly more uniform than 2% APTES. 2% APTES, DSB, and SAV functionalized glass (E) as compared to 5% APTES, DSB, and SAV functionalized glass (F). Both glass surfaces were initially oxygen plasma cleaned prior to functionalization. The heights shown below correspond to the heights sampled across the red line above. This shows that the fully functionalized 2% APTES is much more uniform than the fully functionalized 5% APTES surface.

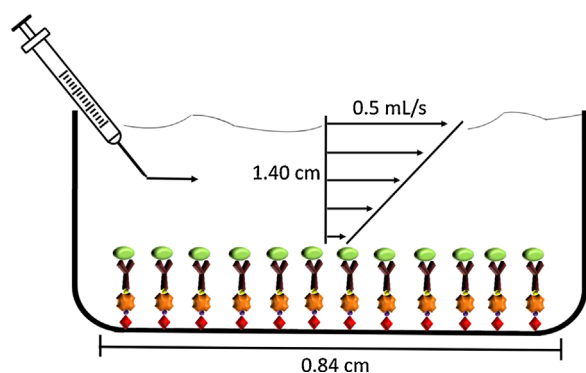


**Figure 5.** Diagram of shear stress calculation on SAV bonding. Shear stress is calculated assuming that the area is  $0.7 \text{ cm}^2$ , that the washing step takes 2 s, and that there is approximately 1 mL of solution in the well. This shows that the wash steps are insufficient to rupture the SAV bond to either DSB or biotin. Scale bar is  $200 \mu\text{m}$  (microns).

MCF7-GFP cells in the unwashed control system as indicated by the fluorescent signal (Fig. 7A) corresponding to 50% cell capture on the surface. However, this non-specific MCF7-GFP adhesion was decreased by 80% when the cells were washed with HBSS. The CD11b facilitates the binding of macrophages, as shown by the merged bright field and widefield microscopy imaging, showing non-fluorescent cells (Fig. 7). There was an  $\sim 80\%$  decrease in the cell capture following 20 min 20 mM biotin incubation. While these results indicate effective cell capture and cell release via the biotin tethering mechanism, the HBSS-mediated cell release suggests antibody tethering may not be highly specific.

## DISCUSSION

Cell separation facilitates the study of structure-function relationships in neuroscience (Drenan et al., 2008), stem cell programming in regenerative biology, and angiogenic signaling in vascular biology (Imoukhuede et al., 2013). However, current cell separation methods can damage cell structure. Systems are needed that can quickly and efficiently isolate specific cell types without disrupting cell-surface receptor levels. To meet these cell isolation challenges we have advanced a new methods in surface functionalization, which (1) creates a system of reliable capture of a single cell type from a mixture of cell types; (2) allows for the gentle and reproducible release of cells; and (3) raises the possibility of capturing different cell types in stages using specific antibodies (Fig. 8).

### SAV Layer Optimization

Surface uniformity is vital to the functionalization of the surface, as non-uniformity results in a decrease in the capture efficiency of the overall surface. In order to improve the surface uniformity, we optimized the concentration of APTES as well as the concentration of DSB. The  $0.3 \text{ mg/mL}$  and  $0.5 \text{ mg/mL}$  concentrations of SAV resulted in large amounts of non-uniformity across the surface of the glass. We chose  $0.4 \text{ mg/mL}$  as it had the lowest non-uniformity

of the concentrations tested. Other concentrations of SAV have been used for surface functionalization. While this concentration is optimal for our application, there is not a consensus as to which concentration is the optimum for maximum uniformity. Indeed, prior SAV functionalization studies have used concentrations ranging from  $5 \mu\text{g/mL}$  to  $10 \text{ mg/mL}$  (Bashir et al., 2001; Nelson et al., 2001; Hirsch et al., 2002; Holmberg et al., 2005; Su et al., 2005; Esseghaier et al., 2008; Lagunas et al., 2010).

### AFM Measurement of Functionalized Surface Height

AFM provides a useful tool for characterizing surfaces (Lee et al., 1994; Cappella and Dietler, 1999; Willemsen et al., 2000; Butt et al., 2005; Williams et al., 2012). In this study, AFM provided insights into both the absolute height of the functionalized surfaces and the surface functionalization variability. When we compared these heights to prior surface functionalization, we observed that the APTES functionalization was within the ellipsometry measured range of  $5.2 \pm 1.8 \text{ nm}$  and the 2% APTES, DSB, and SAV was well within  $9.7 \pm 4.4 \text{ nm}$  (Williams et al., 2012). In addition to height data, we used standard deviation to judge uniformity of the surface. We found that 2% APTES full functionalization produced the least variability in height. These metrics have been used by others to successfully identify surface variation in a variety of materials including orthodontics (D'Antò et al., 2012), thin films (Chen and Huang, 2004), nanofiltration membranes (Boussu et al., 2005), and dentin (El Feninat et al., 2001). We concluded that the 2% APTES fully functionalized was the more uniform surface as it had a lower degree of surface roughness (Fig. 9).

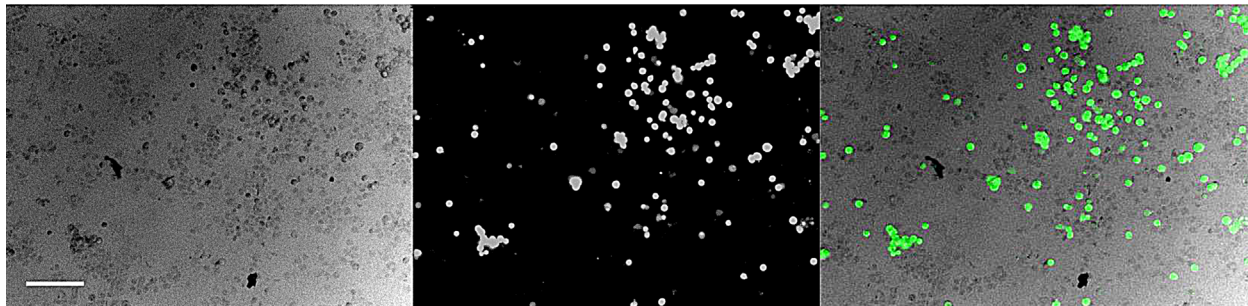
### Applications of AFM

While there are several approaches for AFM-mediated surface imaging (e.g., contact-mode, near contact mode, affinity imaging, etc.), we applied tapping mode for this study, in which, a consistent oscillation directs the tip to tap the surface. Tapping mode imaging is advantageous because it combines near contact and accuracy of reading, without the destructiveness or tip-induced artifacts that can occur when imaging soft materials (Jalili and Laxminarayana, 2004). In addition to our application of tapping AFM to height measurements and uniformity, AFM has successfully been applied towards studying force in biological systems. AFM force measurements can give insight into protein-protein bond breakage. Such force measurements are possible by taking advantage of the fact that AFM measures deflection from the surface, and AFM measures the force that the tip exerts on the surface. This can then be calibrated to measure the amount of force that the substrate places on the tip. These force measurements were particularly insightful in contextualizing the forces required to shear the SAV bonds to DSB and biotin (Lee et al., 2007). These forces gave a valuable starting point for our calculations of whether pipette driven forces were sufficient to shear SAV bonding.

### Importance of Cell Capture and Release

We have established optimized conditions to capture and release cells of interest from a multi-cell population, which is an important

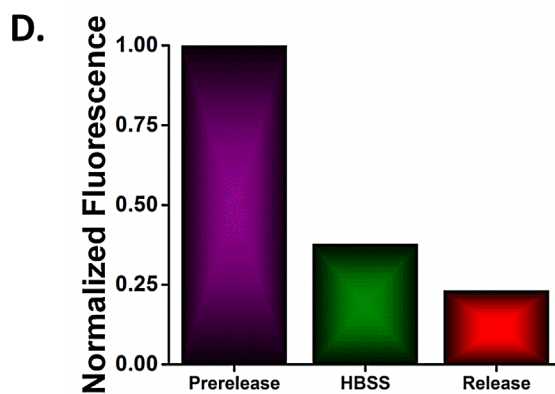
A.



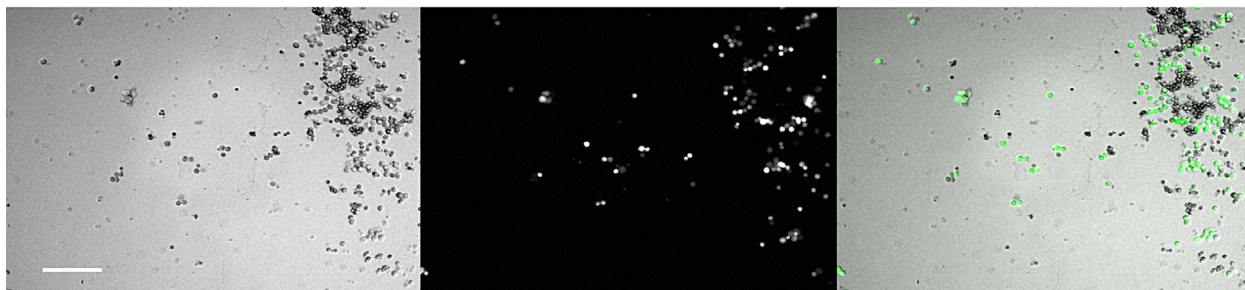
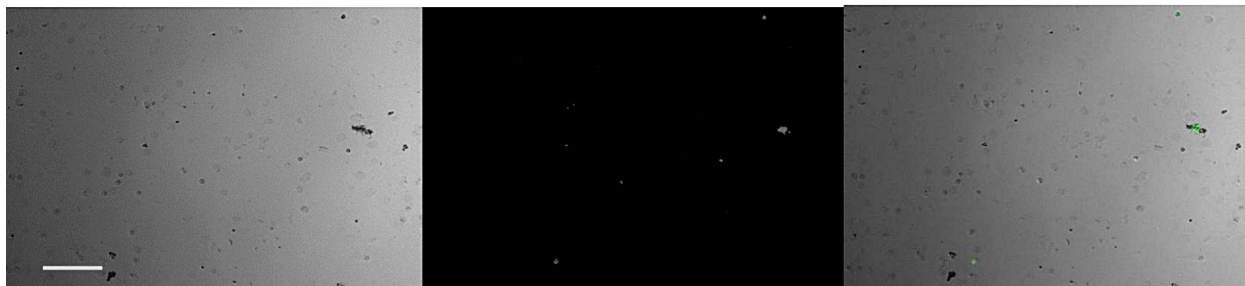
B.



C.



**Figure 6.** Cellular capture of human breast cancer cells (MCF7-GFP) using hIgG antibody on the fully functionalized surface. (A) Captured cells, (B) Cells remaining after HBSS wash (control), (C) Cells remaining after biotin wash (release), and (D) quantification of capture and release fluorescence showing that the fluorescence is substantially reduced when biotin is introduced, as compared with a HBSS wash.

**A****B****C**

**Figure 7.** Cellular capture of cellular mixture containing mouse macrophages (RAW 264.7) and human breast cancer cell line (MCF7-GFP). The mCD11b antibody was used to selectively capture macrophages (A) Cells captured onto the surface, (B) cells remaining after HBSS wash (control), (C) cells remaining after biotin wash (release), showing that the RAW macrophages are preferentially captured and that they are released after addition of biotin. Scale bar is 200  $\mu\text{m}$  (microns).

step towards developing cell isolation paradigms. Cellular separation devices would allow for the quantification of receptor levels (Chen et al., 2014) from a variety of cell types (Yu et al., 2011). Such information can enable the pharmacological or computational modeling that increases efficiency of the targeted treatments; thus, reducing toxicity and even the mortality.

### Current Isolation Limitations

Our system focuses on a secondary anchor targeting release mechanism for the capture and release of cells from a mixed sample. Once functionalized surfaces are developed, the system requires mixing with antibody, surface attachment, and cell removal via biotinylation. We believe that the low number of steps and the gentle approach make it advantageous over some commercially available cell isolation options, which include: Pluribead, and

CELLEX<sup>®</sup>. The pluribead<sup>®</sup> system from Mayflower Biosciences uses a size exclusion filtering system with antigen coated beads (Heinrich and Heinrich, 2012), while the CELLEX<sup>®</sup> from Therakos uses centrifugation, concentrating white blood cells and infusing these white blood cells back into the patients (Perritt et al., 2014). These procedures are personnel limited, thus increasing time, and centrifugation may cause the cell to express different markers or proteins than they would physiologically, which when using this technique for disease monitoring may give false information on progression (Naranbhai et al., 2011). Thus, new methods are necessary that reduce handling.

### Improving Cell Isolation Through Biotin-Avidin Coupling

Our design utilizes DSB-SAv and biotin-SAv interactions, which is commonly used in the biosciences (WIlchek M and Bayer,

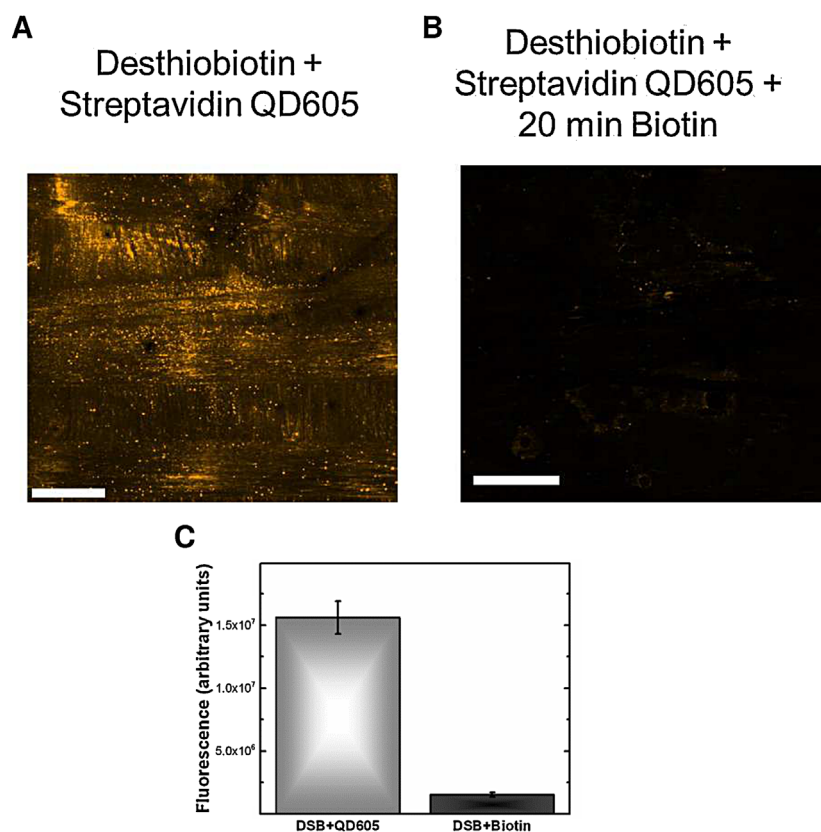


**Figure 8.** Qdot conjugated biotinylated antibodies on the functionalized surface. (A) Captured 605 Qdots, (B) 605 Qdot release: 20 mM biotin solution biotin treatment (C) Comparison of fluorescence showing less fluorescence after application of biotin-showing that the surface has had the functionalized surface removed.

1990; Hirsch et al., 2002). Indeed, the strong, selective binding of the avidin family to the biotin family has been used for over 30 years for a range of scientific and medical applications including: antibody-fluorophore attachment (Wu et al., 2003) and quantitative Qdot-polystyrene bead attachment (Lee-Montiel and Imoukhuede, 2013). Our utilization of DSB for reversible cell attachment has been similarly used with the Dynabead<sup>®</sup> system from Life technologies, which applies DSB-antibodies and magnetic beads for cell separation (Hornes and Korsnes, 1996). However, magnetic isolation can be harsh and result in cellular loss due to the processing steps associated with preparing the samples (Allard et al., 2004; Negrath et al., 2007). Additionally, these processing steps can result in differential receptor and chemokine expression (Negrath et al., 2007; Naranbhai et al., 2011). Furthermore, the use of the beads adds an additional reagent that our surface functionalization overcomes. Therefore, the approach presented here, offers several improvements over prior technology.

### Future Improvements

The technology presented here could be further enhanced by using aptamers rather than antibodies, to tailor it for use with other cell types or for specific applications. Future development of molecules

that are specific to cell types of interest could be integrated to improve the efficiency of the cell capture using this method. A nano-patterning of the surface could also be tested as another method to improve the efficiency by directing the positions of the ligands. This is important in designing a lab on a chip type of system for sequential separation of different cell types at different stages. Integrating microfluidics with our capture surface to create a separation device is another area that could be further optimized in future versions of the technology. The cell viability may be increased by changing the geometry and flow rate of the device. Previous authors have optimized fluid flow and geometries to increase mixing (Winkler et al 2004; Schudel et al 2009; Watkins et al 2013; Gabrielson et al 2013), while others have optimized materials to reduce the cost of production of the device, allowing for the development of diagnostic devices for personalized medicine (Luecha et al 2011).

### CONCLUSION

In summary, novel adhesive ligands combined with creative designs will change the trend of adhesion-based cell sorting devices in the future. There is an immediate need to discover and introduce cell-specific biomolecules to be used in conjunction with cell separation microfluidic devices. A portable, easy-to-use and

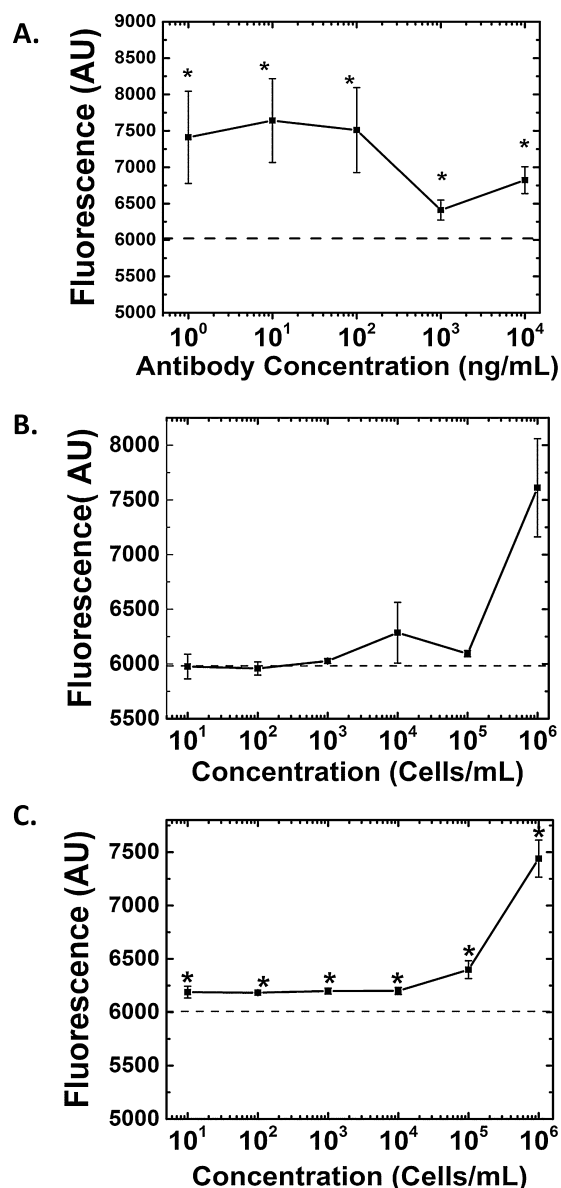


**Figure 9.** Antibody and Cell Saturation Curves of GFP cells plus antibodies bound to a fully functionalized 24-well plate. Antibody saturation curve of HLA (A) showing that concentrations of 10 ng/mL are ideal. The significance is in comparison to the background,  $P < 0.05$ . This concentration was used for the cell saturation and titration experiments. Cell concentrations were kept constant at one million cells/mL. Cellular saturation curve using HLA (B) and hIgG (C) antibodies at 10 ng/mL. The blank (background) is shown on the graph as a dashed line.

inexpensive adhesion-based cell separation microchip can be used in personalized medicine, early stage diagnosis, and in regenerative medicine for separation of tumor cells, stem cells and other rare cell types. This technology would revolutionize personalized medicine and treatment options and improve the physiological relevancy of computational modeling. Additionally, many other applications of this technology can be envisioned for future applications, as this technology can be readily integrated into a variety of existing architectures.

We would like to thank the American Cancer Society, Illinois Division Basic Research Grant and Mexico's National Council of Science and Technology (CONACyT) for funding support. We also would like to thank Scott Maclaren from the Fredrich Seitz Material Research Laboratory for his help with atomic force microscopy and Dianwen Zhang from the Beckman Institute Microscopy Suite for help with fluorescence microscopy. We would like to thank Dr. Kris Kilian as well for his help with discussion on the functionalization procedure. Lastly, we would like to thank Jared Weddell, Stacie Chen, and Spencer Mamer for insightful discussions.

## References

- Allard WJ, Matera J, Miller MC, Repollet M, Connelly MC, Rao C, Tibbe AGJ, Uhr JW, Terstappen LWMM. 2004. Tumor Cells Circulate in the Peripheral Blood of All Major Carcinomas but not in Healthy Subjects or Patients With Nonmalignant Diseases. *Clin Cancer Res* 10(20):6897–6904.
- Arya C, Kralj JG, Jiang K, Munson MS, Forbes TP, DeVoe DL, Raghavan SR, Forry SP. 2013. Capturing rare cells from blood using a packed bed of custom-synthesized chitosan microparticles. *J Mater Chem B* 1(34):4313–4319.
- Asahara T, Murohara T, Sullivan A, Silver M, van der Zee R, Li T, Witzenbichler B, Schatteman G, Isner JM. 1997. Isolation of Putative Progenitor Endothelial Cells for Angiogenesis. *Science* 275(5302):964–966.
- Bashir R, Gomez R, Sarikaya A, Ladisch MR, Sturgis J, Robinson JP. 2001. Adsorption of avidin on microfabricated surfaces for protein biochip applications. *Biotechnol Bioeng* 73(4):324–328.
- Boussu K, Van Der Bruggen B, Volodin A, Snauwaert J, Van Haesendonck C, Vandecasteele C. 2005. Roughness and hydrophobicity studies of nanofiltration membranes using different modes of AFM. *J Colloid Interface Sci* 286(2):632–638.
- Butt H-J, Cappella B, Kappl M. 2005. Force measurements with the atomic force microscope: Technique, interpretation and applications. *Surf Sci Rep* 59(1):1–152.
- Caicedo HM, Dempere LA, Vermerris W. 2012. Template-mediated synthesis and bio-functionalization of flexible lignin-based nanotubes and nanowires. *Nanotechnology* 23(10):105605.
- Cappella B, Dietler G. 1999. Force-distance curves by atomic force microscopy. *Surf Sci Rep* 34(1):1–104.
- Chen Y, Huang W. 2004. Numerical simulation of the geometrical factors affecting surface roughness measurements by AFM. p 2005-2010.
- Chen Si, Ali Ansari, William Sterrett, Kate Hurley, Jeremy Kemball, Jared Weddell, I PI. 2014. Current State-of-the-Art and Future Directions in Systems Biology. *Prog Commun Sci*.
- Chen S, Guo X, Imarenezo O. 2015. Quantitation of VEGFRs, NRP1, and PDGFRs on endothelial cells and fibroblasts reveals serum, intra-family ligand, and cross-family ligand regulation. *Cell Mol Bioeng*.
- Cheung LSL, Zheng X, Stopa A, Baygents JC, Guzman R, Schroeder JA, Heimark RL, Zohar Y. 2009. Detachment of captured cancer cells under flow acceleration in a bio-functionalized microchannel. *Lab Chip* 9(12):1721–1731.
- Cristofanilli M, Budd GT, Ellis MJ, Stopeck A, Matera J, Miller MC, Reuben JM, Doyle GV, Allard WJ, Terstappen LWMM, et al. 2004. Circulating Tumor Cells, Disease Progression, and Survival in Metastatic Breast Cancer. *N Engl J Med* 351(8):781–791.
- D'Antò V, Rongo R, Ametrano G, Spagnuolo G, Manzo P, Martina R, Paduano S, Vallettae R. 2012. Evaluation of surface roughness of orthodontic wires by means of atomic force microscopy. *Angle Orthodontist* 82(5):922–928.
- De Coppi P, Bartsch G, Jr, Siddiqui MM, Xu T, Santos CC, Perin L, Mostoslavsky G, Serre AC, Snyder EY, Yoo JJ, et al. 2007. Isolation of amniotic stem cell lines with potential for therapy. *Nat Biotech* 25(1):100–106.
- Doroshov J. 2009. In: Institute NC, editor. NCI's Roadmap to Personalised Cancer Treatment. Department of Health and Human Services: National Cancer Advisory Board: U.S.
- Drenan RM, Nashmi R, Imoukhuede P, Just H, McKinney S, Lester HA. 2008. Subcellular Trafficking, Pentameric Assembly, and Subunit Stoichiometry of Neuronal Nicotinic Acetylcholine Receptors Containing Fluorescently Labeled  $\alpha 6$  and  $\beta 3$  Subunits. *Mol Pharmacol* 73(1):27–41.

- Dreus-Elger K, Brinkman J, Miller P, Shah S, Harrell JC, da Silva T, Ao Z, Schlater A, Azzam D, Diehl K, et al. 2014. Primary breast tumor-derived cellular models: Characterization of tumorigenic, metastatic, and cancer-associated fibroblasts in dissociated tumor (DT) cultures. *Breast Cancer Res Treat* 144(3):503–517.
- El Feninat F, Elouatik S, Ellis TH, Sacher E, Stangel I. 2001. Quantitative assessment of surface roughness as measured by AFM: Application to polished human dentin. *Appl Surf Sci* 183(3-4):205–215.
- Essegheier C, Bergaoui Y, Ben Fredj, Helali A, Ameer S, Abdelghani S. 2008. Impedance spectroscopy on immobilized streptavidin horseradish peroxidase layer for biosensing. *Sensor Actuat B-chem* 134(1):112–116.
- Ferrara N, Kerbel RS. 2005. Angiogenesis as a therapeutic target. *Nature* 438(7070):967–974.
- Galletti G, Sung MS, Vahdat LT, Shah MA, Santana SM, Altavilla G, Kirby BJ, Giannakakou P. 2014. Isolation of breast cancer and gastric cancer circulating tumor cells by use of an anti HER2-based microfluidic device. *Lab Chip* 14(1):147–156.
- Gascoyne PRC, Noshari J, Anderson TJ, Becker FF. 2009. Isolation of rare cells from cell mixtures by dielectrophoresis. *Electrophoresis* 30(8):1388–1398.
- Hansen C. 2015. Personalized Medicine: The Future of Cancer Care. In: CAN) ACSCANA, editor. *CANCER CANDOR: A blog from the ACS CAN President: American Cancer Society Cancer Action Network (ACS CAN)*.
- He L, Kniss A, San-Miguel A, Rouse T, Kemp ML, Lu H. 2015. An automated programmable platform enabling multiplex dynamic stimuli delivery and cellular response monitoring for high-throughput suspension single-cell signaling studies. *Lab Chip* 15(6):1497–1507.
- Heinrich HW, Heinrich JM. 2012. Method for Separating Particles and/or Cells Having 2 and More Surface Specificities. Google Patents.
- Hirsch JD, Eslamizar L, Filanoski BJ, Malekzadeh N, Haugland RP, Beechem JM, Haugland RP. 2002. Easily reversible desthiobiotin binding to streptavidin, avidin, and other biotin-binding proteins: Uses for protein labeling, detection, and isolation. *Anal Biochem* 308(2):343–357.
- Hoffmann M, Müller W, Ringsdorf H, Rourke AM, Rump E, Suci PA. 1992. Molecular recognition in biotin-streptavidin systems and analogues at the air-water interface. *Thin Solid Films* 210–211, Part 2(0):780–783.
- Holmberg A, Blomstergren A, Nord O, Lukacs M, Lundeberg J, Uhlén M. 2005. The biotin-streptavidin interaction can be reversibly broken using water at elevated temperatures. *ELECTROPHORESIS* 26(3):501–510.
- Hornes E, Korsnes L. 1996. Oligonucleotide-linked magnetic particles and uses thereof. Google Patents.
- Imoukhuede PI, Popel AS. 2011. Quantification and cell-to-cell variation of vascular endothelial growth factor receptors. *Exp Cell Res* 317(7):955–965.
- Imoukhuede PI, Popel AS. 2012. Expression of VEGF receptors on endothelial cells in mouse skeletal muscle. *PLoS One* 7(9):e44791.
- Imoukhuede PI, Popel AS. 2014. Quantitative fluorescent profiling of VEGFRs reveals tumor cell and endothelial cell heterogeneity in breast cancer xenografts. *Cancer Med* 3(2):225–244.
- Imoukhuede PI, Dokun AO, Annex BH, Popel AS. 2013. Endothelial cell-by-cell profiling reveals temporal dynamics of VEGFR1 and VEGFR2 membrane-localization following murine hindlimb ischemia. *Am J Physiol Heart Circ Physiol* 4(8):H1085–H1093.
- Jalili N, Laxminarayana K. 2004. A review of atomic force microscopy imaging systems: Application to molecular metrology and biological sciences. *Mechatronics* 14(8):907–945.
- Kelly OG, Chan MY, Martinson LA, Kadoya K, Ostertag TM, Ross KG, Richardson M, Carpenter MK, D'Amour KA, Kroon E, et al. 2011. Cell-surface markers for the isolation of pancreatic cell types derived from human embryonic stem cells. *Nat Biotech* 29(8):750–756.
- Kuzuya A, Numajiri K, Kimura M, Komiyama M. 2008. Single-Molecule Accommodation of Streptavidin in Nanometer-Scale Wells Formed in DNA Nanostructures. *Nucleic Acids Symp Ser* 52(1):681–682.
- Lagunas A, Comelles J, Martínez E, Samitier J, Martínez E. 2010. Universal Chemical Gradient Platforms Using Poly(methyl methacrylate) Based on the Biotin–Streptavidin Interaction for Biological Applications. *Langmuir* 26(17):14154–14161.
- Lee GU, Kidwell DA, Colton RJ. 1994. Sensing discrete streptavidin-biotin interactions with atomic force microscopy. *Langmuir* 10(2):354–357.
- Lee C-K, Wang Y-M, Huang L-S, Lin S. 2007. Atomic force microscopy: Determination of unbinding force, off rate and energy barrier for protein-ligand interaction. *Micron* 38(5):446–461.
- Lee-Montiel FT, Imoukhuede PI. 2013. Engineering quantum dot calibration standards for quantitative fluorescent profiling. *J Mater Chem B* 1(46):6434.
- Lien K-Y, Chuang Y-H, Hung L-Y, Hsu K-F, Lai W-W, Ho C-L, Chou C-Y, Lee G-B. 2010. Rapid isolation and detection of cancer cells by utilizing integrated microfluidic systems. *Lab Chip* 10(21):2875–2886.
- Liu L, Louterback K, Liao D, Yeater D, Lambert G, Estevez-Torres A, Sturm JC, Getzenberg RH, Austin RH. 2010. A microfluidic device for continuous cancer cell culture and passage with hydrodynamic forces. *Lab Chip* 10(14):1807–1813.
- Ludwig A, Kretzmer G, Schügerl K. 1992. Determination of a “critical shear stress level” applied to adherent mammalian cells. *Enzyme Microb Technol* 14(3):209–213.
- Magalhães MLB, Czekster CM, Guan R, Malashkevich VN, Almo SC, Levy M. 2011. Evolved streptavidin mutants reveal key role of loop residue in high-affinity binding. *Protein Sci* 20(7):1145–1154.
- Mantovani A, Sozzani S, Locati M, Allavena P, Sica A. 2002. Macrophage polarization: Tumor-associated macrophages as a paradigm for polarized M2 mononuclear phagocytes. *Trends Immunol* 23(11):549–555.
- Mishra A, Kwon J-S, Thakur R, Woreley S. 2014. Optoelectrical microfluidics as a promising tool in biology. *Trends Biotechnol* 32(8):414–421.
- Murdoch C, Giannoudis A, Lewis CE. 2004. Mechanisms regulating the recruitment of macrophages into hypoxic areas of tumors and other ischemic tissues. 2224–2234 p.
- Nagrath S, Sequist LV, Maheswaran S, Bell DW, Irimia D, Utkus L, Smith MR, Kwak EL, Digumarthy S, Muzikansky A, et al. 2007. Isolation of rare circulating tumour cells in cancer patients by microchip technology. *Nature* 450(7173):1235–1239.
- Naranbhai V, Bartman P, Ndlovu D, Ramkalawon P, Ndung'u T, Wilson D, Altfeld M, Carr WH. 2011. Impact of blood processing variations on natural killer cell frequency, activation, chemokine receptor expression and function. *J Immunol Methods* 366(1-2):28–35.
- Nelson KE, Gamble L, Jung LS, Boeckl MS, Naeemi E, Golledge SL, Sasaki T, Castner DG, Campbell CT, Stayton PS. 2001. Surface Characterization of Mixed Self-Assembled Monolayers Designed for Streptavidin Immobilization. *Langmuir* 17(9):2807–2816.
- Park K, Akin D, Bashir R. 2007. Electrical capture and lysis of vaccinia virus particles using silicon nano-scale probe array. *Biomed Microdevices* 9(6):877–883.
- Perritt D, Wong P, Macpherson JL, Henrichsen K, Symonds G, Pond S. 2014. Processing blood. Google Patents.
- Plouffe BD, Brown MA, Iyer RK, Radisic M, Murthy SK. 2009. Controlled capture and release of cardiac fibroblasts using peptide-functionalized alginate gels in microfluidic channels. *Lab Chip* 9(11):1507–1510.
- Qureshi MH, Wong S-L. 2002. Design, production, and characterization of a monomeric streptavidin and its application for affinity purification of biotinylated proteins. *Protein Expr Purif* 25(3):409–415.
- Roxworthy BJ, Johnston MT, Lee-Montiel FT, Ewoldt RH, Imoukhuede PI, Toussaint KC, Jr. 2014. Plasmonic Optical Trapping in Biologically Relevant Media. *PLoS ONE* 9(4):e93929.
- Salwitz JC. 2012. The Future is Now: Personalized Medicine. In: Society AC, editor. *Expert Voices: Timely insight on cancer topics from the experts of the American Cancer Society: American Cancer Society*.
- Schudel BR, Choi CJ, Cunningham BT, Kenis PJA. 2009. Microfluidic chip for combinatorial mixing and screening of assays. *Lab Chip* 9(12):1676–1680.
- Sheng W, Ogunwobi OO, Chen T, Zhang J, George TJ, Liu C, Fan ZH. 2014. Capture, release and culture of circulating tumor cells from pancreatic cancer patients using an enhanced mixing chip. *Lab Chip* 14(1):89–98.
- Stott SL, Hsu C-H, Tsukrov DI, Yu M, Miyamoto DT, Waltman BA, Rothenberg SM, Shah AM, Smas ME, Korir GK, et al. 2010. Isolation of circulating tumor cells using a microvortex-generating herringbone-chip. *Proc Natl Acad Sci* 107(43):18392–18397.
- Su X, Wu Y-J, Robelek R, Knoll W. 2005. Surface Plasmon Resonance Spectroscopy and Quartz Crystal Microbalance Study of Streptavidin Film Structure Effects on Biotinylated DNA Assembly and Target DNA Hybridization. *Langmuir* 21(1):348–353.

- Tanzeglock T, Soos M, Stephanopoulos G, Morbidelli M. 2009. Induction of Mammalian Cell Death by Simple Shear and Extensional Flows. *Biotechnol Bioeng* 104(2):360–370.
- Wilchek M, Bayer EA. 1990. Applications of avidin-biotin technology: Literature survey. San Diego, CA, ETATS-UNIS. Elsevier. 32.
- Weddell JC, Imoukhuede PI. 2014. Quantitative Characterization of Cellular Membrane-Receptor Heterogeneity through Statistical and Computational Modeling. *PLoS ONE* 9(5):e97271.
- Willemsen OH, Snel MM, Cambi A, Greve J, De Grooth BG, Figdor CG. 2000. Biomolecular interactions measured by atomic force microscopy. *Biophys J* 79(6):3267–3281.
- Williams EH, Davydov AV, Motayed A, Sundaresan SG, Bocchini P, Richter LJ, Stan G, Steffens K, Zangmeister R, Schreifels JA. 2012. Immobilization of streptavidin on 4H-SiC for biosensor development. *Applied surface science* 258(16):6056–6063.
- Winkler CM, Rani SL, Vanka SP. 2004. Preferential concentration of particles in a fully developed turbulent square duct flow. *Int J Multiphase Flow*, 30(1), 27–50. doi:10.1016/j.ijmultiphaseflow.2003.11.003
- Wu X, Liu H, Liu J, Haley KN, Treadway JA, Larson JP, Ge N, Peale F, Bruchez MP. 2003. Immunofluorescent labeling of cancer marker Her2 and other cellular targets with semiconductor quantum dots. *Nat Biotech* 21(1):41–46.
- Yu M, Stott S, Toner M, Maheswaran S, Haber DA. 2011. Circulating tumor cells: Approaches to isolation and characterization. *J Cell Biol* 192(3):373–382.
- Yu M, Ting DT, Stott SL, Wittner BS, Ozsolak F, Paul S, Ciciliano JC, Smas ME, Winokur D, Gilman AJ, et al. 2012. RNA sequencing of pancreatic circulating tumour cells implicates WNT signalling in metastasis. *Nature* 487(7408): 510–513.
- Zheng X, Cheung LS-L, Schroeder JA, Jiang L, Zohar Y. 2011. A high-performance microsystem for isolating circulating tumor cells. *Lab Chip* 11(19):3269–3276.

## Supporting Information

Additional supporting information may be found in the online version of this article at the publisher's web-site.